A theoretical analysis of mercury molecules*

Earl W. Smith, R. E. Drullinger, M. M. Hessel, and J. Cooper†

Laser Physics Section, National Bureau of Standards, Boulder, Colorado 80302
(Received 10 January 1977)

A theoretical analysis of experimental observations on bound–free electronic transitions in mercury molecules is presented. Potential curves and A values are derived for these transitions and the possibility of emission from a mercury trimer is also discussed briefly. These data are then used to produce a theoretical model for an optically pumped 335 nm mercury laser. A table is given which predicts the small signal gain at 335 nm as a function of temperature, density, and the excimer density in the vapor.

I. INTRODUCTION

The Hg_2 molecule is representative of a class of molecules, often known as excimer molecules, which have dissociative ground states and bound excited states. Such molecules are of interest as possible high power visible or ultraviolet lasers because they avoid the lower state bottleneck which often inhibits electronic transition lasers. Owing to the lack of a bound ground state, standard absorption techniques cannot be used to obtain the molecular structure parameters needed for modeling laser systems. We have therefore developed new measurement techniques (both experimental and theoretical) to obtain potential curves, transition rates, and various kinetic rates for this class of molecules. The experimental measurement techniques and their application to mercury vapor are discussed by Drullinger *et al.*[1] In the present paper we will discuss the theoretical analysis of the data thus obtained. In particular, we derive radiative transition rates, potential curves for the ground state and several excited states of Hg_2, and also give a brief discussion of the possibility of emission from a mercury trimer. We also present parameters for design of an optically pumped Hg_2 excimer laser.

The data analyzed in this paper consist of both fluorescence and absorption data. The fluorescence measurements[1] used the 257.2 nm frequency doubled argon laser line as an optical pump and the steady state fluoresence signal was measured from 240 nm to 650 nm with a resolution of 20 nm (spectra obtained with higher resolution are also discussed in Ref. 1). Measurements were made for temperatures from 573 to 1273 K for atomic densities ranging from 10^{16} cm^{-3} to 2.2×10^{19} cm^{-3}. Three representative spectral traces are shown in Figs. 1, 2, and 3. In general, one sees two strong molecular bands centered roughly at 335 and 500 nm; the latter will be referred to as the 485 band to be consistent with previous literature on mercury. At low densities there is also a significant signal from the very broad red wing of the collision broadened 253.7 nm ($^3P_1$–$^1S_0$) atomic transition. In Fig. 1, the pump laser was focused to a rather small beam diameter resulting in a power density the order of 1.5 W/cm^2. This produced some two photon excitation of the $7\,^3S_1$ atomic state as well as a rather strong scattering of the 257.2 nm pump laser and the 514.5 nm primary laser. In later data the pump laser was not tightly focused and very little if any double pumping was observed; in addition, the 257.2 and 514.5 nm laser scattering were greatly reduced (owing to improved light baffles, etc.).

As mentioned earlier, the absorption measurements are quite difficult, requiring pressures in the range of one or more atmospheres, long absorption path lengths (e.g., 80 cm), and temperatures the order of 900–1300 K. Kuhn and Freudenberg[2] have measured the absorption spectrum photographically, and Drullinger *et al.*[1] have measured the temperature and density dependence of the absorption coefficient photoelectrically at several key wavelengths.

In Sec. II we discuss the theoretical basis for our analysis of the spectral data. In Secs. III and IV these techniques are applied to the 335 and 485 bands, respectively. In Sec. V we discuss parameters for design of an optically pumped laser.

II. METHOD OF ANALYSIS

A. General features

Expressions for spontaneous emission, absorption, and stimulated emission in excimers are derived in the Appendix using the assumptions that (1) the excited

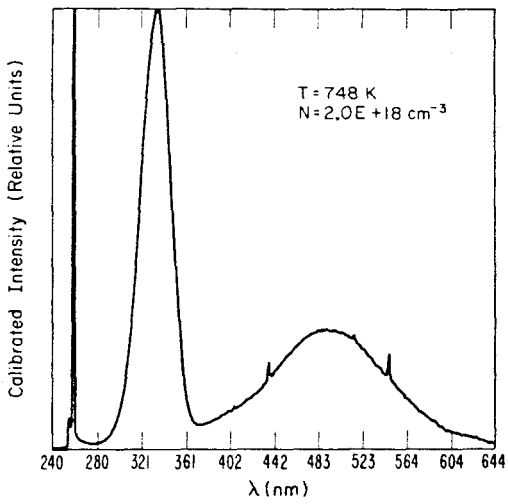

FIG. 1. Relative photon flux[26] vs wavelength. The primary features are the molecular bands at 335 and 485 nm, the 253.7 nm atomic line with its strong red wing due to collision broadening, strong scattering of the 257.2 nm pump laser, a weak feature at 514.5 nm due to scattering of the argon ion laser which was frequency doubled to produce the pump laser, and weak atomic emission $^3S_1 - {}^3P_{0,1,2}$ at 404.6, 435.8, and 546.0 nm due to two photon pumping of higher lying states.

state well depth is much greater than kT, (2) the vibrational spacing is much less than kT, and (3) the ground state well depth (if any) is shallow enough that the number of bound ground state molecules is much less than the number of atoms. Similar theoretical descriptions have been developed by Hedges *et al.*,[4] Doyle,[5] and Sando and Dalgarno.[6] Throughout this section we will make a distinction between the excited state vibrational temperature T_a and the gas temperature T even though these two temperatures will be equal for all of the data analyzed in the present paper. This distinction will make the equations more general and permit them to be used for the analysis of molecules excited by electrical discharges (see, for example, Mosburg and Wilke[7]).

The number of photons emitted into 4π steradians is

$$I(\lambda)\,d\lambda = A_{ab}(R_\lambda)\,\phi(\lambda)\,\frac{n_a \exp[-V_a(R_\lambda)/kT_a]}{\Lambda_a^3 q_a}\left(\frac{c}{\lambda^2}\right)d\lambda\,, \tag{2.1}$$

where a and b denote excited and ground states, respectively, and T_a is the vibrational temperature of the excited state. A_{ab} is an A value defined by

$$A_{ab}(R_\lambda) = \frac{64\pi^4\nu^3}{3hc^3}\,g_b\left|D_{ab}(R_\lambda)\right|^2\,, \tag{2.2}$$

where $D_{ab}(R_\lambda)$ is the electronic transition dipole matrix element evaluated at the internuclear separation R_λ at which the radiative transition takes place (according to the Franck–Condon principle), and g_b is the electronic degeneracy of the ground state b. Other quantities appearing in Eq. (2.1) which refer to the electronic state a are n_a, the density of excimers in the state a, the rotation–vibration partition function q_a, the potential energy $V_a(R)$ as a function of internuclear separation ($V_a = 0$ at the bottom of the excited state well), and a thermal de Broglie wavelength

$$\Lambda_a = \sqrt{h^2/2\pi\mu kT_a}\,, \tag{2.3}$$

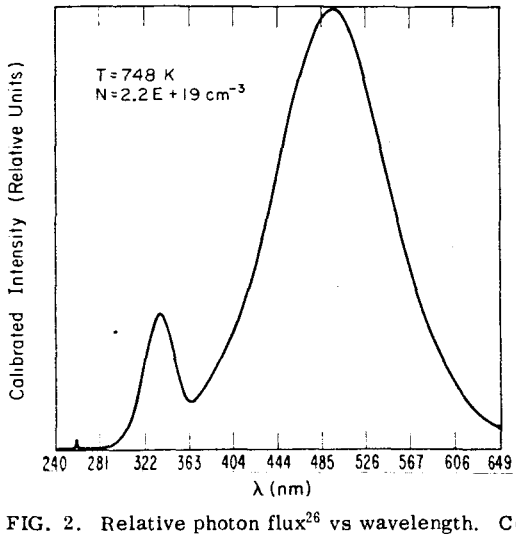

FIG. 2. Relative photon flux[26] vs wavelength. Comparison with Fig. 1 shows that increasing the density increases the 485 nm molecular band intensity and decreases the intensity of the 253.7 nm atomic line relative to the 335 nm molecular band (see also Figs. 5 and 8). The laser scatter and two photon pumping are also strongly reduced owing to the use of a slightly wider laser beam (i.e., decreased power density).

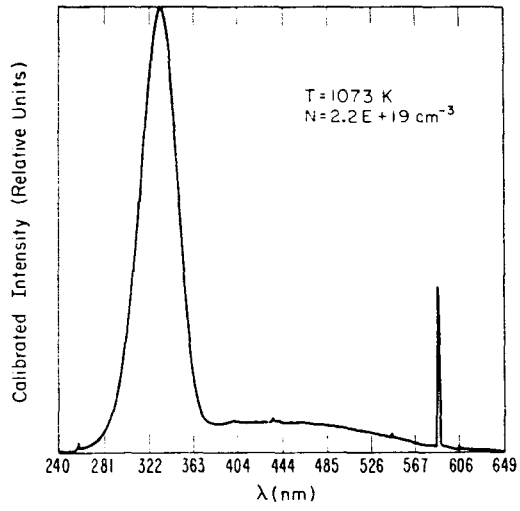

FIG. 3. Relative photon flux[26] vs wavelength. Comparing with Fig. 2 shows that an increase in temperature strongly increases the ratio of 335 to 485 nm molecular band intensities (see also Fig. 4). The intensity of the 253.7 nm laser line decreases slightly with temperature, but this is shown more clearly in Fig. 9. Atomic sodium lines at 589.0 and 589.6 nm (merged into a single feature by the 2.0 nm spectral resolution) are also present since the rather high temperature causes sodium atoms to be ejected from the glass cell walls.

in which μ is the reduced mass of the molecule (e.g., 1.7×10^{-22} g for Hg_2). The line shape function $\phi(\lambda)$ is defined by (see Appendix)

$$\phi(\lambda) = 4\pi R_\lambda^2\left[\frac{d}{dR}\left(\frac{V_a(R_\lambda) - V_b(R_\lambda)}{h}\right)_{R=R_\lambda}\right]^{-1}\,, \tag{2.4}$$

where $V_b(R)$ is the potential energy of the ground state $V_b(R)\to 0$ as $R\to\infty$.

The absorption coefficient defined by $dI(\lambda, x)/dx = I(\lambda, x)k(\lambda)$ is

$$k(\lambda) = \left(\frac{\lambda^2}{8\pi}\right)A_{ab}(\lambda)\,\phi(\lambda) \times\left[\frac{g_a n^2}{g_b}\,e^{-V_b(R_\lambda)/kT} - \left(\frac{n_a}{\Lambda_a^3 q_a}\right)e^{-V_a(R_\lambda)/kT_a}\right]\,, \tag{2.5}$$

where T is the gas temperature, n is the ground state atom density, g_a is the electronic degeneracy of the excited state, and the negative term represents stimulated emission. It should be noted that our line shape function $\phi(\lambda)$ is not normalized although one can easily define normalized emission and absorption line profiles (see Appendix).

One can obtain a simple classical picture of Eqs. (2.1)–(2.4) by assuming that the number of photons emitted in a radiative transition is given by the product of an A value $A(R)$, a delta function $\delta\{h\nu - E_a - V_a(R) + V_b(R)\}$ which selects photons of wavelength λ (E_a denotes the energy of the bottom of the excited state well relative to the energy of a ground state atom), and the probability of finding the molecule at the internuclear distance R:

$$P(R)\,dR = 4\pi R^2\,e^{-V_a(R)/kT_a}\,dR/Z_a\,, \tag{2.6}$$

$$Z_a = \int 4\pi R^2\,e^{-V_a(R)/kT_a}\,dR\,. \tag{2.7}$$

$I(\lambda)$ is then given by

$$I(\lambda)\,d\lambda = n_a\left(\frac{cd\lambda}{\lambda^2}\right)\int A_{ab}(R)\,\delta(h\nu - E_a - V_a(R) + V_b(R)) \times \frac{4\pi R^2 e^{-V_a(R)/kT}}{Z_a}\,dR$$

$$= n_a\left(\frac{cd\lambda}{\lambda^2}\right)\frac{A_{ab}(R_\lambda)}{Z_a}\,e^{-V_a(R_\lambda)/kT_a}\,\frac{4\pi R_\lambda^2}{h(d\nu/dR)_{R=R_\lambda}}$$

$$= n_a\left(\frac{cd\lambda}{\lambda^2}\right)\frac{A_{ab}(R_\lambda)}{Z_a}\,\phi(\lambda)\,e^{-V_a(R_\lambda)/kT_a}\,, \qquad (2.8)$$

where the point R_λ is defined by

$$h\nu = E_a + V_a(R_\lambda) - V_b(R_\lambda)\,. \qquad (2.9)$$

The classical limit of the partition function is given by

$$q_a = \sum_{vJ}(2J+1)\,e^{-E_{vJ}/kT} = h^{-3}\int d^3p\int d^3R\,e^{-V_a(R)/kT_a}e^{-p^2/2mkT_a}$$

$$= \Lambda_a^{-3}Z_a\,. \qquad (2.10)$$

With this expression Eq. (2.8) becomes identical to Eq. (2.1), thereby showing how $I(\lambda)$ and $k(\lambda)$ may be obtained when a classical description of the molecule is valid.

Occasionally a case will arise where the spectrum due to one electronic transition overlaps with that of another. For example, the 485 and 335 fluorescence bands overlap around 400 nm and two overlapping absorption bands are discussed in Sec. III.A. In such cases there will be more than one value of R corresponding to a given wavelength λ and it is necessary to sum the right hand side of Eqs. (2.1) and (2.5) over R_λ.

Equations (2.1) and (2.5) were derived under the assumption that the vibration–rotation levels are in thermal equilibrium within a given electronic state (the various electronic states need not be in thermal equilibrium, of course). Our first measurements were therefore intended to determine the conditions under which this assumption is valid. We first plotted the ratio of integrated band intensities for the 485 and 335 nm fluoresence bands as a function of gas temperature and density (Figs. 4–6). For densities greater than 3×10^{17} cm^{-3} and temperatures greater than 575 K, the log of this ratio is a linear function of $1/kT$ and the 6500 cm^{-1}

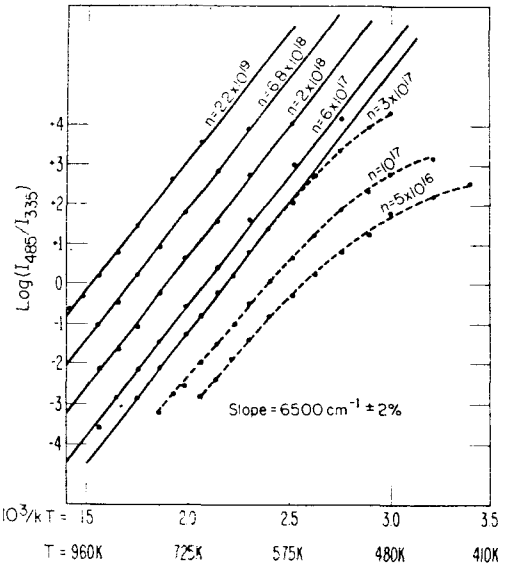

FIG. 4. Ratio of integrated band intensities versus temperature for several different densities (in cm^{-3}). All of these data are calibrated so that the ratio gives the number of photons emitted in the 485 band divided by the number emitted in the 335 band. This ratio can be fit by the function $2.2\times10^{-24}n \times \exp(6500/kT)$, where kT is in cm^{-1} [see Eq. (4.10)].

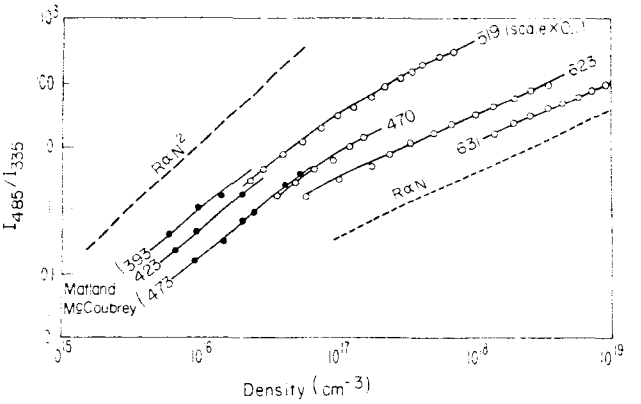

FIG. 5. Ratio of integrated band intensities vs density for several different temperatures (in degrees Kelvin). These data were obtained using optical filters and are thus not calibrated in terms of photon flux as are the data of Fig. 4. The data at 519 K have been shifted upward 1 order of magnitude in order to clarify the figure. The low temperature data of Matland and McCoubrey[25] are also included to show that this ratio approaches an n^2 dependence.

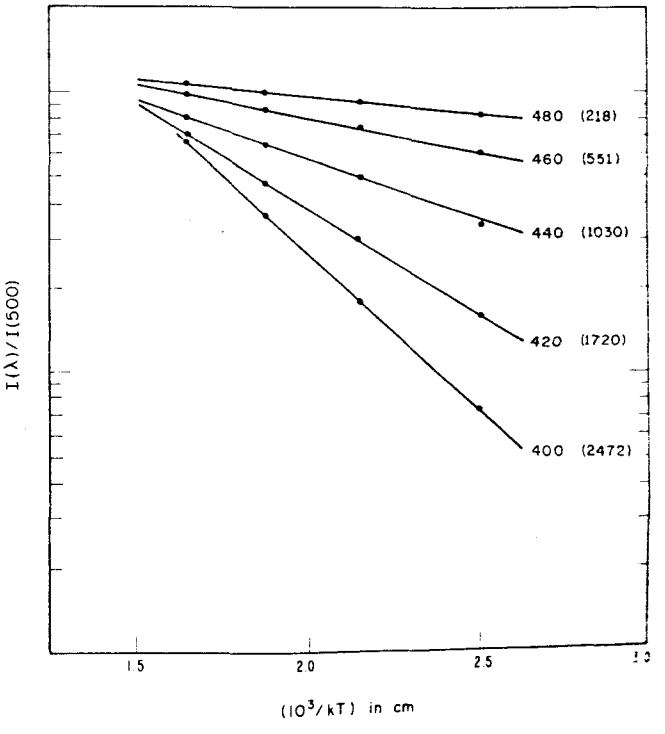

FIG. 6. Ratio of intensities at various wavelengths λ in the 485 band relative to the intensity at 500 nm. Each plot is labeled by the wavelength λ and, in parentheses, its slope. The slope of each plot is equal to its energy, in cm^{-1}, relative to the energy of the state which emits at 500 nm.

slope is independent of density. This shows that the ratio of populations is indeed described by a Boltzmann factor and it also shows that the states which emit the 485 and 335 nm bands are separated by 6500 cm^{-1} in energy.

Figure 5 shows that for the higher temperatures and densities where thermal equilibrium applies, the ratio of 485 and 335 nm bands is a linear function of gas density. If the 335 nm band is due to spontaneous emission from an Hg_2 dimer (as we have shown by measuring its density dependence in absorption), then the 485 nm must result from an Hg_3 complex. The latter could be either be a bound trimer or an unbound complex which could be referred to as collision induced dimer emission. This question will be discussed further in Sec. IV.

B. Fluorescence analysis

Having shown that the two different electronic states responsible for the prominent fluorescence bands were in thermal equilibrium when $n > 3\times10^{17}$ cm^{-3} and $T > 575$ K, we proceeded to make $\log[I(\lambda)/I(\lambda')]$ vs $1/kT$ plots for various wavelengths within the 485 and 335 bands. The log of this ratio is (notice that n_a and the partition functions cancel out)

$$\log\left(\frac{I(\lambda)}{I(\lambda')}\right) = \frac{V_a(R_{\lambda'}) - V_a(R_\lambda)}{kT} + \log\left[\left(\frac{\lambda'}{\lambda}\right)^2 \frac{A_{ab}(\lambda)\phi(\lambda)}{A_{ab}(\lambda')\phi(\lambda')}\right] . \quad (2.11)$$

Thus, if we plot $\log I(\lambda)/I(\lambda)$ vs $1/kT$, the slope of the linear plot will give the relative potentials $V_a(R_{\lambda'}) - V_a(R_\lambda)$ and the infinite temperature intercept will give the relative $A\phi$ values. By doing this for several values of λ, for a fixed λ', we can plot out V_a as a function of wavelength. For example, when studying the 485 band we use $\lambda' = 500$ nm since we always have a strong signal at this wavelength. Figure 6 shows a semilog plot of $I(\lambda)/I(500))$ vs $1/kT$ for several wavelengths in the 485 band; the number in parentheses gives the slope in cm^{-1}. The excellent linearity of these plots shows that the vibrational states are in thermal equilibrium as one would expect. These data, and several more sets, which we have not plotted, have been analyzed by a linear least squares computer program to obtain the slopes. The relative $A\phi$ values, $A_{ab}(\lambda)\phi(\lambda)/A_{ab}(500)\phi(500)$, are obtained from the $(1/kT) = 0$ intercept of the plot. Since a small error in the slope can produce a large variation in the zero intercept, the $A\phi$ values are less accurate than the potentials themselves.

This simple method works rather well when one band dominates over all others. This method has been used by Drullinger *et al.*[8] to evaluate the potential curves (upper and lower states) for the 335 band from 300 to 360 nm and for the 485 band from 400 to 600 nm. Overlap of the 485 and 335 bands prevented us from going to longer wavelengths in the 335 band and to shorter wavelengths in the 485 band. Extension of the 335 band to shorter wavelengths is complicated by overlap with the red wing of the collision broadened 253.7 nm atomic line. Extension of the 485 band to longer wavelengths was inhibited[8] by blackbody radiation from the oven, but this has been eliminated[1] by chopping the optical pump and using synchronous detection of the fluorescence.

C. Two density method for fluorescence

A slightly more sophisticated method has been developed which extends the 335 band to the range 280–370 nm with an order of magnitude increase in accuracy over the region 300–360 nm. Similarly, the 485 band is extended to 350–360 nm again with an order of magnitude increase in accuracy over 400–600 nm.

This technique makes use of the fact that, for $n > 10^{17}$ cm^{-3}, the ratio of integrated band intensities, $I(485)/I(335)$, is proportional to the vapor density (see Fig. 5). If $I(\lambda, n, T)$ represents the number of photons emitted at wavelength λ, density n, and temperature T, then we may define

$$I(\lambda, n, T) = \frac{\alpha(n, T)}{\lambda^2}\left[A_1(\lambda)\phi_1(\lambda)\, e^{-E_1(\lambda)/kT} + n\, a_1(\lambda)\phi_2(\lambda)\, e^{-E_2(\lambda)/kT}\right] , \quad (2.12)$$

$$\alpha(n, T) = n_a/\Lambda_a^3 q_a , \quad (2.13)$$

where the subscripts 1 and 2 denote the contributions from the electronic states responsible for the 335 and 485 bands, respectively. Note that the A value for the 485 band, $a_2(\lambda)$, does not have the same units as $A_1(\lambda)$; this is due to the fact that $a_2(\lambda)$ also includes the rate of formation for the Hg_3 complex which radiates the 485 band.

In the region where the bands overlap, both terms in Eq. (2.12) must be retained; however, in the center of the bands we may write

$$I(335, n, T) = \alpha\lambda^{-2} A_1(335)\phi_1(335)\, e^{-E_1(335)/kT} ,$$
$$I(500, n, T) = \alpha\lambda^{-2} n\, a_2(500)\phi_2(500)\, e^{-E_2(500)/kT} . \quad (2.14)$$

It is thus clear that an expression such as

$$\frac{I(\lambda, n_1, T)}{I(335, n_1, T)} - \frac{I(\lambda, n_2, T)}{I(335, n_2, T)} = \left(\frac{500}{\lambda}\right)^2 (n_1 - n_2)\, \frac{a_2(\lambda)\phi_2(\lambda)}{A_1(335)\phi_1(335)} \exp\left(\frac{E_1(335) - E_2(\lambda)}{kT}\right) \quad (2.15)$$

contains no contribution from the state $E_1(\lambda)$ (i.e., the 335 band); hence it is possible to obtain the 485 potential curves [by plotting the log of Eq. (2.15) vs $1/kT$] even in a region where the 335 band is stronger. In practice this technique works until the 335 band is about 2 orders of magnitude stronger than the contribution from the 485 band; at that point, the 1% noise level on the total signal produces an error in the subtraction of the 335 contribution which is almost as large as the 485 signal. The same technique can be used to extend the potential curves for the 335 band by using $I(500, n, T)$ in the denominator.

III. 335 BAND

A. Absorption data

Figure 7 shows the low lying Hg_2 curves as well as some key radiative transitions which are used to locate

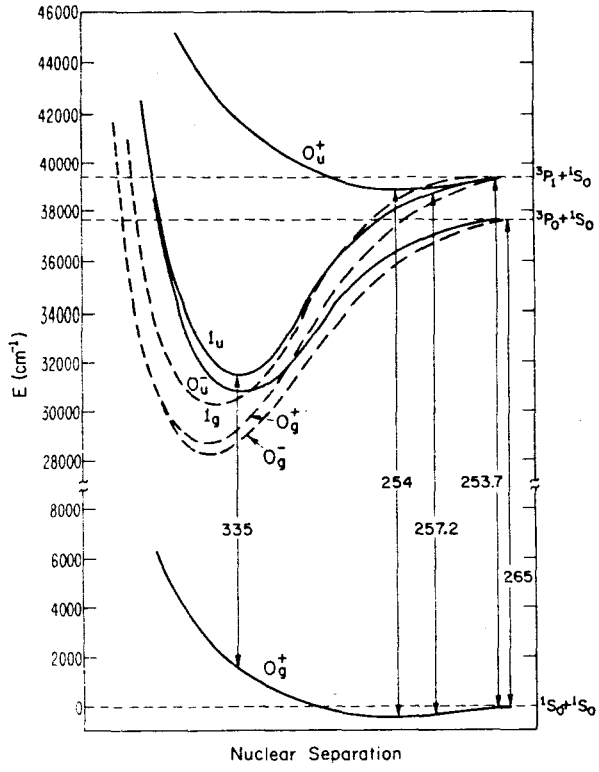

FIG. 7. Theoretical estimates of several low lying Hg_2 potential curves based on *ab initio* calculations of Mg_2 and experimental observations on Hg_2 (Stevens[9] and Mies *et al.*[6]). They are intended to show (1) the relative energy ordering of the states. (2) the relative values of R_e (i.e., the internuclear separations at the bottoms of the various wells), (3) the convergence of the 0_u^- and 1_u states at small internuclear distances. and (4) the approximate magnitude of the splitting between gerade and ungerade states.

the energies of various ungerade states. The locations of the gerade states are not firmly established and are at present only estimates based on *LS* splittings in the atomic states. The two lowest excited states which can make allowed transitions to the ground state are the 1_u and the 0_u^+. On purely theoretical grounds (Stevens[9] and Mies *et al.*[10]), the 0_u^+ is expected to be weakly bound whereas the 1_u is strongly bound. Consequently, the 335 mm band (which is observed to go as n^2 in absorption) is ascribed to the 1_u.

In studying the absorption spectrum, it was found that the absorption coefficient $k(\lambda)$ was proportional to n^2 (for all cases where two photon pumping was absent, see Ref. 1, Sec. III]. It was also found [by plotting the log of $k(\lambda)$ vs $1/kT$] that the absorption coefficients at 257.2 and 265 nm could not be described by a single Boltzmann factor. This is not surprising since the 0_u^+ state should have an A value slightly larger than that for the 1_u state [due to its greater admixture of singlet character (Stevens[9] and Mies *et al.*[10])]; consequently, the absorption coefficient should be a sum of two terms

$$k(\lambda) = n^2(k_0 e^{-E_0/kT} + k_1 e^{-E_1/kT}) , \qquad (3.1)$$

where the subscripts 0 and 1 refer to the $0_g^+ - 0_u^+$ and $0_g^+ - 1_u$ transitions, respectively. Using this functional form we obtained excellent fits to the 257.2 and 265 nm data, the results of which are given in Table I. Notice that transitions to the 0_u^+ state correspond to points rather high up the repulsive wall of the 0_g^+ ground state. For the $\lambda > 265$ nm data, $E_0 \gg E_1$ and the contribution from transitions to the 0_u^+ state were too weak to be measured (i.e., only the k_1 term was measured). Comparing Eq. (3.1) with Eq. (2.5) and noting that $g_a = 2$ and $g_b = 1$, we see that $k_1 = (\lambda^2/4\pi) A_{ab}(\lambda)\phi(\lambda)$; the measured values of the product $A\phi$ are also given in Table I.

B. Fluorescence data

The molecular fluorescence data analyzed in this paper were excited with the 257.2 nm frequency doubled output of a 514.5 nm argon laser line. As shown in Fig. 7, this laser line excites vibrational levels of the 1_u state which lie above the $^3P_0$ atomic level. This highly excited 1_u molecule can predissociate, via curve merging with the 0_u^- at small R, into a $6\,^3P_0 + 6\,^1S_0$ atom pair. The metastable $^3P_0$ atom (natural lifetime $\simeq 1$ sec) then acts as an energy reservoir and feeds excitation into the various Hg_2^* states by three-body recombination processes. This pumping scheme has been verified (for densities greater than 2×10^{18} cm^{-3}) by exciting with a 5 nsec laser pulse at 256 nm (obtained from the frequency doubled output of a nitrogen pumped dye laser). The strong fluorescence near the laser pump frequency was observed to decay in less than 1 nsec (the limit of our time resolution) after the exciting pulse was turned off. A weak fluorescence signal coincident in time with the laser pulse was observed at all wavelengths in the 335 nm band, indicating that there was some collisional redistribution of the directly pumped 1_u states while the laser pulse was on. However, the dominant molecular fluorescence turned on rather slowly (100 nsec rise-time) following the laser pulse, indicating that most of the laser excitation was converted into $^3P_0$ metastable atoms as stated above.

TABLE I. Summary of absorption measurements and the upper states assigned to them. All energies are in cm^{-1}, and $A\phi$ is in cm^3. The tabulated ground state energy refers to the energy at the point R_λ where the radiative transition takes place. Data for transitions to 0_u^+ are rather noisy owing to an insufficient range in temperature ($T \gg 900$ C would be needed) and the steepness of the exponentials $\exp(-V/kT)$. We were unable to obtain reasonable estimates of $A\phi$ for the $0_g \rightarrow 0_u^+$ transition owing to the rather large uncertainty in the ground state energy. The accuracy of the 1_u energies is the order of ± 100 cm^{-1}.

λ(nm)	Ground state energy	Excited state energy	$A(\lambda)\phi(\lambda)$
257.2 (0_u^+)	+3800 ± 1500	42 680 ± 1500	Uncertain
257.2 (1_u)	−150	38 730	7.3×10^{-29}
265 (0_u^+)	+6900 ± 3000	44 640 ± 3000	Uncertain
265 (1_u)	−255	37 480	9.9×10^{-30}
280 (1_u)	−170	35 544	2.37×10^{-30}
313.1 (1_u)	+550	32 487	4.20×10^{-31}
334. (1_u)	+1600	31 540	1.87×10^{-31}

The fluorescence data for the 335 band were analyzed by both methods discussed in the previous section (Secs. II. B and II. C). It was found that the two density method was effective in removing the contribution due to the 485 nm band on the long wavelength side of the 335 nm band. Our analysis of the long wavelength side was restricted only when the ratio of 485 to 335 contributions became comparable to the signal to noise ratio of the data (see discussion in Sec. II. C).

On the short wavelength side of the 335 band, we began to notice a deviation from linearity in the $\log[I(\lambda)/I(\lambda')]$ vs $1/kT$ plots for $\lambda < 280$ nm which became rather severe as one approached the 253.7 nm line. It was also clear that the region from 253.7 to 280 nm did not have the same density dependence as the 335 band. Plots were made of $I(262)/I(336)$ as a function of density, Fig. 8, and it was found that this ratio approached a $1/n$ dependence at low n. This same behavior was observed at other wavelengths in the 253.7–280 nm range, with the $1/n$ behavior becoming less pronounced as one approached the 335 nm band (since the contribution due to the latter becomes dominant). This radiation is probably due to overlap with the red wing of the collision broadened 253.7 nm line (see Fig. 9) with perhaps an additional contribution near 265 nm due to collision induced radiation from $^3P_0$ atoms. The latter process could occur when $^3P_0$ and $^1S_0$ atoms approach one another along the 0_u^- curve (see Fig. 7), cross over to the 1_u curve at small R, and subsequently find themselves quasibound in the 1_u state. Radiation could then occur from the outer turning point at 265 nm and from the inner turning point at some longer wavelength as yet unobserved. In either case, these radiators are not expected to be in thermal equilibrium with the vibrational states at the bottom of the 1_u well (which emit at 335 nm). This is due to the fact that the bottom of the 1_u curve is separated by the order of 6500 cm^{-1} from the $^3P_0$ atomic level, and the collision rate upwards, $nv\sigma \exp(-6500/kT)$, cannot compete with radiative losses from the 1_u state (using $v\sigma \simeq 10^{-10}$ cm^3 sec^{-1} and $A \simeq 10^6$ sec^{-1}).

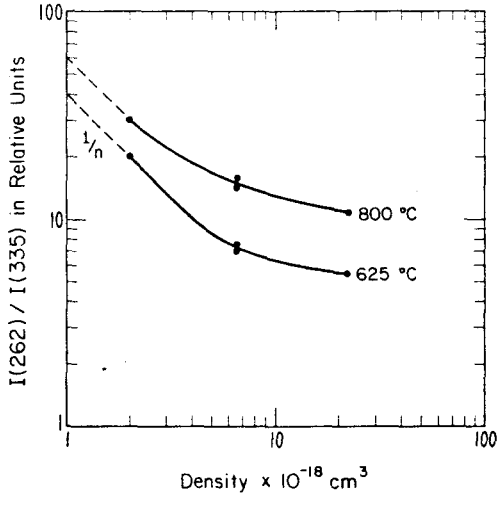

FIG. 8. Fluorescence intensity at 262 nm relative to that at 335 nm vs density for two representative temperatures. This plot is intended to show the behavior of the relative intensities of the collision broadened 253.7 atomic line wing and the 335 nm molecular band. At low densities this ratio is no longer independent of density, indicating that the radiators which emit at 262 nm (i.e., collision broadened 6^3P atoms) are not in thermal equilibrium with the bottom of the 1_u state in Hg_2.

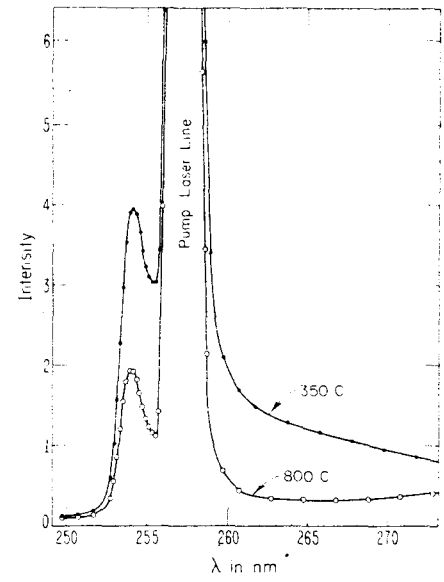

FIG. 9. Fluorescence intensity at a density of 2×10^{18} cm^{-3} for the temperatures 800 °C and 350 °C showing the extensive red wing of the 253.7 nm atomic line. Any structure due to self-reversal at the line center is smeared out due to the 2.0 nm resolution of the spectrometer.

Having thus obtained some idea as to the source of the radiation in the 253.7–280 nm region, we attempted to remove its effect by the two density method. This was not successful because there was too large a contribution from the 335 nm band in the vicinity of 254 nm (see Sec. II. C). Consequently, we have reported results only for $\lambda > 280$.

The potential curves $V(\lambda)$ and transition probabilities $A(\lambda)\phi(\lambda)$ were evaluated over the range 280–370 nm with points every 0.2 nm; hence there are 450 data points for each function. It is therefore convenient to represent these functions by the polynomials

$$E_1(\lambda) = 31500 + V(\lambda)\ , \tag{3.2}$$

$$V(\lambda) = 0.3106\Delta\lambda + 1.457\Delta\lambda^2 + 6.329\times10^{-3}\Delta\lambda^2 + 1.877 \times10^{-4}\Delta\lambda^4 + 1.968\times10^{-6}\Delta\lambda^5 - 1.731\times10^{-8}\Delta\lambda^6\ , \tag{3.3}$$

$$A(\lambda)\phi(\lambda) = 3.23\times10^{-31}(313.1\ \text{nm}/\lambda)^3\,(0.9169 - 1.099 \times10^{-2}\Delta\lambda - 1.158\times10^{-4}\Delta\lambda^2 + 5.851\times10^{-6}\Delta\lambda^3 + 3.512\times10^{-7}\Delta\lambda^4 - 1.456\times10^{-8}\Delta\lambda^5 - 2.725 \times10^{-10}\Delta\lambda^6\ \text{cm}^3), \tag{3.4}$$

where $\Delta\lambda = (\lambda - 340\ \text{nm})$, λ is expressed in nm, $V(\lambda)$ expresses the 1_u potential energy in cm^{-1} relative to $V(340) = 0$, which is the bottom of the well, and $E_1(\lambda)$ is the absolute potential energy (i.e., the energy relative to a ground state atom). The absolute scaling of the data in Eqs. (3.2) and (3.4) was determined by comparison with the absorption measurement at 313.1 nm. That is, Eq. (3.2) gives a ground state energy $E_1(\lambda) - h\nu_\lambda$ of

TABLE II. Summary of data for transitions involving the 1_u excited state. The internuclear distance R is given in atomic units and angstroms (the latter in parentheses). Energies are given in cm^{-1}, $A\phi$ is in cm^3, the A value is in sec^{-1}, and the transition dipole D is in debyes. Absorption data are marked with an asterisk.

λ(nm)	R	Ground state	Excited state	$A(\lambda)\phi(\lambda)$	A	D
257.2*	9.00 (4.76)	−150	38730	7.30×10^{-29}		
265.*		−255	37480	9.90×10^{-30}		
280*	6.22 (3.29)	−170	35544	2.37		
285	6.12 (3.24)	−0.5	35087	1.37	2.94×10^{6}	0.46
290	6.03 (3.19)	143	34625	1.19	4.65	0.59
295	5.98 (3.17)	226	34124	9.68×10^{-31}	7.64	0.78
300	5.95 (3.15)	290	33624	7.60	6.59	0.74
305	5.92 (3.13)	364	33151	5.94	4.08	0.60
310	5.88 (3.11)	447	32725	4.74	2.39	0.47
313.1*	5.84 (3.09)	550	32487	4.20		
315	5.83 (3.08)	610	32356	3.93	1.51	0.38
320	5.76 (3.05)	800	32051	3.41	1.27	0.36
325	5.70 (3.01)	1042	31812	3.07	1.03	0.33
330	5.62 (2.97)	1337	31640	2.80	8.58×10^{5}	0.31
334*	5.56 (2.94)	1600	31540	1.87		
335	5.55 (2.94)	1685	31536	2.55	8.30	0.31
340	5.48 (2.90)	2090	31502	2.31	7.34	0.30
345	5.40 (2.86)	2555	31541	2.08	6.07	0.28
350	5.33 (2.82)	3088	31659	1.86	6.07	0.28
355	5.26 (2.78)	3698	31867	1.66	5.32	0.27
360	5.19 (2.74)	4399	32177	1.47	4.54	0.26
365	5.11 (2.70)	5210	32608	1.20	3.69	0.24
370	5.04 (2.66)	6154	33181	7.30×10^{-32}	2.44	0.20

550 cm^{-1} at $\lambda = 313.1$ nm and $A(\lambda)\phi(\lambda) = 4.20\times10^{-31}$ at 313.1 cm^{-1} (see Table I). We expect the relative values of the potential function to be accurate to within 30 cm^{-1}, and the absolute energy $E_1(\lambda)$ should be accurate to within 50 cm^{-1}. The absolute value of the product $A(\lambda)\phi(\lambda)$ is accurate to within about 10% and the relative values of $A\phi$ should be accurate to within about 2%, except near 280 nm, where there may be a larger error due to overlap with the wing of the 253.7 nm atomic line.

C. Radial scaling

The potential $V(\lambda)$ should be sufficient for laser modeling purposes; however, it is also interesting to have $V(R)$ for comparison with *ab initio* potential surfaces, etc. We have therefore applied a radial scale using the pseudopotential calculations of Baylis and Walornyj[11] for the Hg_2 ground state. At each wavelength, we first determined the ground state energy for the transition. We then assigned that transition to the internuclear distance R which gave the same ground state energy in the Baylis–Walornyj calculation. The results, including both fluorescence and absorption data, are tabulated in Table II and are plotted in Fig. 10. When the ground state energy is negative, the assignment of R is not unique since there are two points, namely, the inner and outer turning points, which have the same ground state energy. For the fluorescence measurements at 280 and 257.2 nm, we simply chose the most reasonable values of R by comparing with the rest of the excited state data. For the absorption at 265 nm, neither the inner nor the outer turning point gave good agreement with the rest of the excited state data. However, the potential is very flat in this region and a 200 cm^{-1} error in either the measurement or the theoretical ground state well depth could shift the value of R by the order of an angstrom. In this connection, it should be noted that the calculated well depth is 440 cm^{-1}, whereas an analysis of experimental data by Kuhn[12] gives an uncertainty of 530 $cm^{-1} < D_0 < 740$ cm^{-1} and our measurement (Sec. V or Ref. 1) gives 460 cm^{-1}, in agreement with the value 480 cm^{-1} obtained by Frank and Grotrian[13] and by Koernieke.[14] Thus we are at present unsure of the actual ground state well depth.

In Fig. 10, we have plotted the C_6/R^6 asymptotes obtained from line broadening studies of the far wings of the 253.7 nm line $6\,^3P_1$–$6\,^1S_0$ by Kuhn[12] and by Perrin–Lagarde and Lennuier.[15] Kuhn points out that one must be very careful in extracting the C_6 coefficient for the excited state since both $^3P_0$ and $^3P_1$ states contribute. The relationship between the C_6^0 and C_6^1 coefficients is not known at present, hence one can only obtain upper and lower bounds for their values. In Fig. 10 we have therefore plotted C_6^1/R^6 for the maximum and mimimum values of C_6^1 obtained from Kuhn's data (the data of Perrin-Legarde and Lennuier give a slightly lower maximum value, but the minimum value is unchanged). In general, one would expect the true $V(R)$ to approach the C_6 asymptote from below, and our $V(R)$ satisfies this condition.

The excited state potential curve evaluated in this manner has been approximated by a Hulbert–Hirschfelder potential function which gave a vibrational frequency the order of 150 cm^{-1} and a rotational constant of 0.02 cm^{-1}.

The potential curves $V(R)$ must be regarded as very

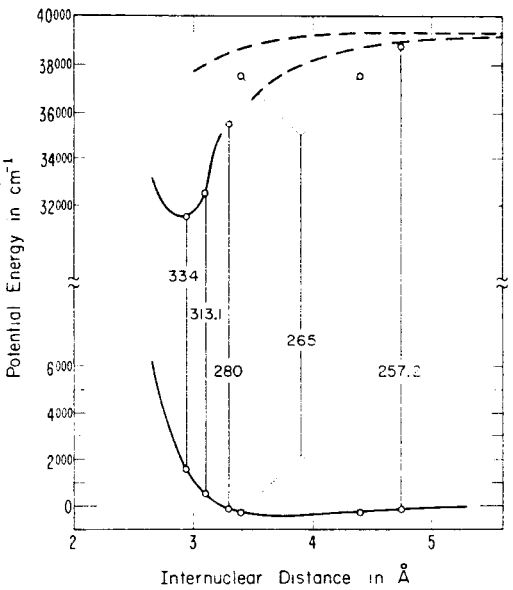

FIG. 10. Ground state and 1_u excited state potential curves as functions of internuclear distance. The ground state is obtained from the pseudopotential calculation of Baylis and Wolornyj. The dashed curves represent the upper and lower bounds on the C_6/R^6 asymptote for the 1_u state obtained from the data of Kuhn. The solid excited state curve is obtained from our fluorescence data and the open circles denote our absorption measurements. The radial scale for our absorption and fluorescence data was obtained by choosing the value of R in the Baylis–Wolornyj calculation which gave the same ground state energy as the measurement for each wavelength plotted. When the ground state energy is negative there are two possibilities, namely, the inner and outer turning points, and we simply chose the point which gave the most reasonable result. For the absorption at 265 nm neither point gave very good agreement with the rest of the excited state data; however, the ground state potential is very flat in this region and 200 cm^{-1} uncertainty in either the measurement or the theoretical well depth could change the 265 nm point by the order of an angstrom.

approximate since the radial scaling is based on a pseudopotential calculation which is surely in error by some unknown amount. On the other hand, these curves are instructive since they do give some idea of the relative behavior of the 1_u state as a function of R, and the comparison with C_6^1/R^6 indicates that our curves are physically quite reasonable.

With an approximate $V(R)$ in hand it is now possible to evaluate the line shape function $\phi(\lambda)$ defined in Eq. (2.4) and thus obtain the A value for the transition as well as the transition dipole moment from Eq. (2.2). Table II contains the dipole moment as a function of internuclear separation as well as the A value. These quantities are subject to considerable error since they rely on the radial derivative of the potential difference function and small errors in $V(R)$ will be magnified by the derivative. We thus expect that the A value and the transition dipole $D(R)$ are accurate to within a factor of 2 or so.

It is interesting to note that while the bottom of the excited state well lies at about 340 nm, the peak emission occurs near 335 nm (depending on temperature). This is due to the fact that the product $A\phi$ increases with decreasing λ and I_λ is proportional to $\lambda^{-2}A\phi$. For the same reason, the emission peak is observed to shift toward shorter wavelengths as the temperature is increased (i.e., as the population is shifted higher in the 1_u well). On the other hand, the gain coefficient is proportional to $\lambda^2 A\phi$, which means that the peak of the gain curve will lie slightly closer to 340 nm. For practical lasers, however, the temperature will be rather high (see Sec. V), so the peak will again move back near 335 nm.

IV. 485 BAND

At low temperatures and high pressures there is a very broad emission band centered (after correcting for the spectrometer and phototube response curves) at 500 nm. This band is usually called the 485 band because uncalibrated spectral data tend to peak at 485 nm. When discussing this band it is important to keep in mind the fact that the response of phototubes falls off exponentially as one goes to red wavelengths and it is necessary to calibrate the spectral data before one knows what the actual band shape looks like. For example, it is often thought that this band cuts off at about 550 nm, yet our calibrated spectral (Fig. 2) show that there is appreciable intensity even beyond 600 nm.

As already mentioned, the ratio of 485 to 335 nm band intensities increases linearly with the atom density n in the temperature–density range ($T > 575$ K, $n > 3\times10^{17}$ cm^{-3}), where these two electronic states are known to be in thermal equilibrium (Fig. 5). The 335 nm band is known to come from Hg_2 (since it goes as n^2 in absorption); thus the 485 nm band could arise from either a stable Hg_3 molecule or a collision induced complex involving a metastable state of Hg_2 which is induced to radiate when perturbed by a collision. In the latter case the radiation occurs when the atom–molecule interaction breaks the molecular symmetries (e.g., gerade $\not\rightarrow$ gerade or $+\not\rightarrow+$ etc.) which forbid radiation. The situation may be summarized by the equations

$$[Hg_2^*]+[X]-[Hg_2X^*]-2[Hg]+[X]+h\nu_{485}\,, \tag{4.1}$$

$$[Hg_2^*]-2[Hg]+h\nu_{335}\,, \tag{4.2}$$

$$I_{485}/I_{335}\sim[Hg_2^*][X]/[Hg_2^*]=[X]\,, \tag{4.3}$$

where [X] is the ground state atom concentration. If the 485 nm band is due to trimer emission, the atom [X] must be a mercury atom. If this band is due to collision induced emission, the atom–molecule interaction which induces the radiation (e.g., dispersion forces) would not be specific to mercury atoms as perturbers and any atom X should be capable of inducing the radiation. We therefore performed a set of experiments (Sec. II of Ref. 1) using foreign gases to see if the ratio I_{485}/I_{335} would be proportional to the foreign gas atom density (see Sec. II. F of Ref. 1). In all cases this ratio was independent of the foreign gas density, thus arguing in favor of the Hg_3 model for the 485 nm band.

We note also that if the 485 nm radiation were due to the collision induced mechanism, the dimer state involved would most likely be the 0_u^- state (see Fig. 7). Again this makes the collision induced model seem unlikely since the spin–orbit splitting between the 1_u and

O_u^- states is expected to be (Stevens[9] and Mies *et al.*[10]) much less than the 6500 cm^{-1} which is the observed energy spacing between the states radiating the 335 and 485 nm bands (see Fig. 4).

Simple three state kinetic models have been employed in order to test the collision induced hypothesis. Using this hypothesis it has not been possible to explain the observation that $I(485)/I(335)$ is proportional to n for large values of n and rolls over into an n^2 dependence at low n (see Fig. 5). On the other hand, a model invoking 485 nm radiation from a stable trimer does predict this density dependence (due to the extra factor of n required to collisionally stabilize the trimer). In addition, measurements of the long time decay constant (Drullinger *et al.*,[8] Fig. 4.2) have shown an exponential temperature dependence which indicates a thermal destruction of the 485 nm radiator. This would be difficult to interpret in terms of a collision induced complex but it has been successfully modeled in terms of a stable trimer. More detailed kinetic studies are currently in progress and will be reported in a future publication.

In order to defend the trimer model, we must explain the fact that our plots of $\log I(\lambda)/I(500)$ vs $1/kT$ are linear for all values of λ between 350 and 540 nm (i.e., over most but not all of the observed band). This would seem to indicate that (1) the states which radiate the various wavelengths within this band are in thermal equilibrium with one another, and (2) for each wavelength, there is only one energy level which radiates at that wavelength (otherwise we would see a sum of two or more exponentials corresponding to the different energy levels involved). However, a brief consideration of a triatomic potential surface makes it obvious that, owing to the additional degrees of freedom, there will be several states with various energies (i.e., a subset of points on the trimer potential surface) which can radiate at the same wavelength.

For example, let $V_a(r_1\, r_2\, \gamma)$ represent the interaction between the three atoms where $\mathbf{r}_1$ and $\mathbf{r}_2$ denote the positions of two atoms relative to the third, and $\mathbf{r}_1 \cdot \mathbf{r}_2 = \cos\gamma$. As in Eqs. (2.6)–(2.10), the number of emitted photons may be given by

$$I_\lambda d\lambda = n_t \frac{c d\lambda}{\lambda^2} \int dr_1^3 \int dr_2^3 A(r_1\, r_2\, \gamma) \times \delta\{h\nu - \Delta V(r_1\, r_2\, \gamma)\} \frac{e^{-V_a(r_1 r_2 \gamma)/kT}}{Z_a}$$

$$= n_t \frac{c d\lambda}{\lambda^2} 8\pi^2 \int r_1^2 dr_1 \int r_2^2 dr_2 \int d(\cos\gamma) \times A(r_1\, r_2\, \gamma)\, \delta\{h\nu - \Delta V(r_1\, r_2\, \gamma)\} \frac{e^{-V_a(r_1 r_2 \gamma)/kT}}{Z_a}$$

$$= n_t \frac{c d\lambda}{\lambda^2} 8\pi^2 \int dr_1^* \int dr_2^* \times \frac{(r_1^*\, r_2^*)^2 A(r_1^*\, r_2^*\, \gamma^*)\, e^{-V_a(r_1^* r_2^* \gamma^*)/kT}}{Z_a h \left.\frac{d\nu}{d\gamma}\right|_{r_1 r_2 \gamma = r_1^* r_2^* \gamma^*}} , \qquad (4.4)$$

where the locus of points $r_1^*\, r_2^* \gamma^*$ is defined by

$$h\nu = \Delta V(r_1^*\, r_2^* \gamma^*) = E_a + V_a(r_1^*\, r_2^* \gamma^*) - V_b(r_1^*\, r_2^* \gamma^*) . \qquad (4.5)$$

For the dimer, Eq. (2.8), we had only a single point R_λ capable of emitting at wavelength λ (since $V_a - V_b$ is a monotonic function of R). In the case of a trimer we must integrate over a continuous set of points $r_1^* r_2^* \gamma^*$ which can all give rise to photons of wavelength λ. Notice that the final result in Eq. (4.4) is an integral of the general type

$$I = \int_{x_1}^{x_2} f(x)\, e^{-\beta V(x)}\, dx = f(x) \frac{e^{-\beta V(x)}}{\beta} \Big|_{x_2}^{x_1} - \int_{x_1}^{x_2} \frac{df}{dx}\, e^{-\beta V(x)}\, dx , \qquad (4.6)$$

which will be proportional to a sum of two exponentials. In the case of Eq. (4.4), these exponentials are $\exp[-V_{max}(\lambda)/kT]$ and $\exp[-V_{min}(\lambda)/kT]$, where V_{max} and V_{min} are the highest and lowest states which radiate at wavelength λ. If V_{max} is much greater than V_{min} (e.g., 2 or 3 times kT), the contribution from V_{max} would be negligible and we would observe only a single exponential factor. In such a case, the measured $V(\lambda)$ would represent only the state of lowest energy which emits at wavelength λ.

This picture could explain why our plots of $\log(I_\lambda/I_{500})$ vs $1/kT$ are perfectly linear for 340 nm $\leq \lambda \leq$ 540 nm. On the other hand, if there were a region of the potential surface where V_{max} and V_{min} are not very different, we should begin to see a deviation from linearity at high temperatures for values of λ in this region. A deviation from linearity is in fact observed for $\lambda >$ 540 nm, namely, for "internuclear distances" smaller than the equilibrium point (i.e., the bottom of the well). For these wavelengths, we have used only the lower temperatures in determining $V(\lambda)$. We have attempted a two exponential fit to the data in this region but the results did not seem reasonable in terms of our simple trimer models. However, the signal is very weak in this region and a more detailed theoretical study and probably more measurements will be necessary before one can proceed further with the trimer analysis.

As before, it is convenient to present the data in the form of polynomials in λ. These polynomials fit the relative potential energy to within 50 cm^{-1} over the range 350–620 nm, except near the band edges, where overlap with the 335 nm band (blue edge) and loss of photomultiplier sensitivity (red edge) increased fluctuations to ± 100 cm^{-1}. The fit to $A\phi$ is accurate to within $\pm 5\%$ (the noise level of the data). Using eighth order polynomials we obtained

$$E_2(\lambda) = 24\,870 - 3.257\times10^{-2}\Delta\lambda + 9.11\times10^{-2}\Delta\lambda^2 + 2.228\times10^{-4}\Delta\lambda^3 - 1.415\times10^{-5}\Delta\lambda^4 - 1.064\times10^{-7}\Delta\lambda^5 + 1.819\times10^{-9}\Delta\lambda^6 + 1.815\times10^{-11}\Delta\lambda^7 + 4.202\times10^{-14}\Delta\lambda^8 , \qquad (4.7)$$

and

$$a_2(\lambda)\phi_2(\lambda) = 2.17\times10^{-55}\,(500\text{ nm}/\lambda)^3\,(0.7292 - 6.646\times10^{-3}\Delta\lambda + 6.012\times10^{-5}\Delta\lambda^2 - 2.699\times10^{-9}\Delta\lambda^3 - 2.102\times10^{-8}\Delta\lambda^4 + 1.287\times10^{-10}\Delta\lambda^5 + 2.535\times10^{-12}\Delta\lambda^6 - 6.765\times10^{-16}\Delta\lambda^7 - 5.726\times10^{-17}\Delta\lambda^8)\text{ cm}^6\,, \quad (4.8)$$

where $\Delta\lambda = (\lambda - 552\text{ nm})$, λ is in nm, and $E_2(\lambda)$ is the absolute energy in cm^{-1}. The bottom of the trimer well is in the vicinity of 552 nm, but the potential changes very slowly so it is difficult to specify the exact wavelength for the point of lowest energy.

The absolute energy scale, which puts $E_2(552)$ at 24 870 cm^{-1}, was determined by calculating the energy of the dimer state which radiates at 340 nm [whose absolute energy was set at 31 500 cm^{-1} in Eq. (3.2)] relative to the state which radiates at 552 nm. This relative energy, 6629 cm^{-1}, then fixes the absolute energy of $E_2(552)$. The relative energy measurement has an accuracy of about 2%; hence, the absolute energies for the 485 band could be off by the order of 150 cm^{-1}.

The absolute scale for $a\phi$ was determined from the fact that the ratio $I(500)/I(340)$ was observed to go as

$$I(500)/I(340) = 4.72\times10^{-25}\,n\,e^{6500/kT} = n\left(\frac{340}{500}\right)^2\frac{a_2(500)\,\phi_2(500)}{A_1(340)\phi_1(340)} \times\exp\frac{E_1(340) - E_2(500)}{kT}\,, \quad (4.9)$$

where we have used the notation of Eq. (2.14) so that the subscripts 1 and 2 refer to states in the dimer and trimer, respectively. Taking the value of $A_1(340)\phi_1(340)$ from Table II, Eq. (4.9) then provides the scale for the $a_2(\lambda)\phi_2(\lambda)$ values in Eq. (4.8). The accuracy of this scale relies on the measured energy difference $E_1(340) - E_2(500) = 6500\text{ cm}^{-1}$, which is only accurate to within 2%. This error produces an uncertainty the order of 20% in the absolute values of $a(\lambda)\phi(\lambda)$; the relative values across the 485 band should be good to within 5% or 10% as noted above. A list of potential energy functions and "transition probabilities" $a(\lambda)\phi(\lambda)$ for the 485 band is given in Table III.

To avoid confusion it should be noted that the intensities in Eq. (4.9) are measured at a specific wavelength λ whereas the intensities plotted in Fig. 4 are integrated over the entire band. The integrated band intensities are observed to satisfy the equation

$$I_{485}/I_{335} = 2.2\times10^{-24}\,n\,e^{6500/kT}\,. \quad (4.10)$$

Equations (4.9) and (4.10) contain the same exponential factor (i.e., 6500 cm^{-1}) because the points $\lambda = 340$ nm and $\lambda = 500$ nm lie very close to the emission maxima.

One must be careful not to interpret $a(\lambda)$ as an A value since it also contains trimer partition functions, etc. It is possible to obtain an order of magnitude estimate for the trimer A value from the integrated band intensities by assuming that

$$I_{485}/I_{335} = n_2A_{485}/n_1A_{335} = nK_{eq}(T)\,A_{485}/A_{335}\,, \quad (4.11)$$

where the subscripts 1 and 2 again refer to the dimer and trimer, respectively. The A values in this equation are averaged over molecular states weighted (by the vibrational population distribution) strongly toward the band centers.

The equilibrium constant $K_{eq}(T)$ may be estimated by taking the ratio of a typical three-body formation rate $k_2 \simeq 5\times10^{-31}$ cm^6 sec^{-1} to the two-body destruction rate $k_1 \sim 10^{-8}\exp(-6500/kT)$ cm^3 sec^{-1}, the latter being an order of magnitude estimate obtained from our unpublished kinetic data. This ratio gives $K_{eq} \simeq 5\times10^{-23}\exp(6500/kT)$ cm^3. One may also calculate K_{eq} using partition functions (Davidson,[16] pp. 125 and 206). Using a vibrational frequency of 150 cm^{-1} for the dimer and all trimer modes and rotational constants B_e of 0.015 cm^{-1} and 0.008 cm^{-1} for the dimer and trimer, we obtain essentially the same value of K_{eq}. Using this value and equating Eq. (4.11) to Eq. (4.10) gives

$$A_{485} \simeq A_{335}/20\,. \quad (4.12)$$

This gives a value for A_{485} much smaller than one would expect; however, this result is only a crude estimate and may well be off by more than an order of magnitude.

TABLE III. Potential energy and "transition probability" for various wavelengths in the 485 band. Energies are given in cm^{-1} and the units of $a(\lambda)\phi(\lambda)$ are cm^6. Absolute values for the excited and ground state potentials and the transition probabilities $a(\lambda)\phi(\lambda)$ are given as determined in Sec. IV. Values of the excited state potential and the transition probability relative to their values at $\lambda = 550$ are also tabulated.

	Excited state energy			$a(\lambda)\phi(\lambda)$	
λ(nm)	Relative	Absolute	Ground state energy	Relative	Absolute
350	4543	29413	842	170	401.2×10^{55}
360	4013	28883	1105	137	161.7
370	3670	28540	1513	102	120.4
380	3354	28224	1908	78.6	92.8
390	3002	27872	2231	49.2	58.1
400	2604	27474	2474	31.8	37.5
410	2180	27050	2660	19.8	23.4
420	1762	26632	2822	12.0	14.2
430	1377	26247	2991	7.2	8.50
440	1044	25914	3187	4.5	5.31
450	775.1	25645	3423	3.2	3.78
460	568.6	25439	3700	2.6	3.07
470	417.3	25287	4011	2.3	2.71
480	309.1	25179	4346	2.2	2.60
490	230.7	25100	4693	2.1	2.48
500	170.6	25040	5041	2.0	2.36
510	120.5	24990	5383	1.8	2.12
520	76.7	24947	5716	1.6	1.89
530	39.7	24910	6042	1.4	1.65
540	12.8	24883	6364	1.2	1.42
550	0.	24870	6688	1.0	1.18
560	5.6	25430	7573	0.87	1.03×10^{55}
570	28.6	24899	7355	0.76	0.90
580	65.8	24936	7694	0.67	0.79
590	111.6	24982	8032	0.58	0.68
600	162.9	25033	8366	0.51	0.60
610	228.6	25099	8705	0.46	0.54
620	345.1	25215	9086	0.44	0.52

V. PARAMETERS FOR AN OPTICALLY PUMPED LASER

In this section we will consider the conditions necessary for an optically pumped 335 nm laser; the possibility of laser action on the 485 nm band will also be discussed briefly. The gain coefficient for the 335 band is given in Eq. (2.5) as

$$\alpha(\lambda) = \frac{n_a}{\Lambda_a^3 q_a} \frac{\lambda^2}{8\pi} A_{ab}(\lambda)\phi(\lambda)\, e^{-V_a(\lambda)/kT} , \tag{5.1}$$

where the subscripts a and b refer to the excited 1_u and ground 0_g^+ states (see Fig. 7). From Table II we have $A(335)\phi(335) = 2.55\times10^{-31}$ cm^3 and, using $h\nu_{vib} = 150$ cm^{-1} and $B_e = 0.02$ cm^{-1} (see Sec. III.C), the partition functions required by Eq. (5.1) are (see Davidson,[16] p. 125)

$$\begin{aligned} &\Lambda_a = h/\sqrt{2\pi\mu kT} = 5.52\times10^{-10}\sqrt{1000/T}\ \text{cm} , \\ &q_{vib} = kT/h\nu_{vib} = 4.627\,(T/1000) , \\ &q_{rot} = kT/(2.88\,B_e) = 1.21\times10^{4}\,(T/1000) , \\ &\Lambda_a^3 q_a = 9.42\times10^{-24}\ \text{cm}^3\sqrt{T/1000}\ \text{cm}^3 . \end{aligned} \tag{5.2}$$

Using $V_a(335) = 34.2$ cm^{-1} from Table II, the gain at 335 nm is

$$\alpha(335) = 1.2\times10^{-18}\ \text{cm}^3\, n(1_u)\sqrt{T/1000\ \text{K}}\ \exp(-34.2/kT), \tag{5.3}$$

which means that, at $T = 1000$ K, a 1_u density of 10^{14} cm^{-3} will yield about 1%/m gain.

In order to supply this excimer density it is necessary to minimize losses which occur in three major ways. First the power density of the optical pump should be kept as low as possible to minimize two photon excitation of high lying states which is a rather strong effect in the wavelength range 253.7–270.0 nm used for optical pumping (see Sec. IV of Paper I). This means that a high energy pulse of 1–10 μsec duration would be desirable since it is just a bit shorter than the excimer lifetime which is the order of 20–50 μsec depending on the temperature and density [see Fig. (4.2) of Drullinger *et al.*[8]]. Secondly, losses via trimer formation and subsequent 485 band emission should be minimized by operating at low densities and high temperatures. Thirdly, the inversion density should be large enough that ground state absorption is a negligible effect.

It should also be noted that most of the excitation will reside in the low lying metastable 0_g excimers rather than the 1_u state (see Fig. 7). Analysis of the long time decay constant indicates that these gerade states lie about 2500 cm^{-1} below the 1_u [e.g., using the data of Ref. 8, Fig. 4.2), the slope of $\ln(1/\tau)$ vs $1/kT$ is about 2500 cm^{-1}]. If n_{tot} represents the total excimer density and if trimer losses are negligible, the 1_u density will be

$$n(1_u) \simeq n_{tot}\, e^{-2500/kT} . \tag{5.4}$$

Thus it is desirable to operate at as high a temperature as possible in order to minimize the amount of excitation which is "wasted" in the metastable excimer states.

Losses through trimer emission will be less than 10% if $I_{335} \gtrsim 10\, I_{485}$. Using the measured value $I_{485}/I_{335} = 2\times10^{-24}\, n\exp(6500/kT)$, from Eq. (4.10), this condition becomes

$$e^{6500/kT} \gtrsim 5\times10^{22}/n . \tag{5.5}$$

For a density of 5×10^{18} cm^{-3}, for example, this requires the temperature be greater than 1017 K.

The population inversion which results in ground state absorption losses the order of 10% or less is obtained from Eq. (2.5) using the excited and ground state potential energies given in Table II:

$$\frac{2n(1_u)}{\Lambda_a^3 q_a}\, e^{-34/kT} \gtrsim 10 n^2\, e^{-1685/kT} , \tag{5.6}$$

or, using Eqs. (5.2) and (5.4),

$$n(1_u) = n_{tot}\, e^{-2500/kT} \gtrsim 4.7\times10^{-23}\, e^{-1651/kT}\, n^2\sqrt{T/1000\ \text{K}} . \tag{5.7}$$

Notice that the 1_u density, given by the left side of the inequality, and the ground state absorber density, proportional to the right hand side of the inequality, both increase exponentially with temperature. Since the 1_u density increases faster, it will be beneficial to raise the temperature. Increasing the temperature therefore minimizes trimer losses, improves the inversion density, and increases the 1_u population.

We also note that increasing the temperature reduces the amount of energy stored in the $^3P_0$ atomic metastable state. The latter was estimated by integrating the intensity of the 253.7 nm resonance line (whose red wing extends to 280 nm!) and comparing this with the integrated 335 band intensity. Assuming that the $^3P_0$ and $^3P_1$ atomic states are in equilibrium with one another for $n > 3\times10^{17}$ cm^{-3} and $T \gtrsim 1000$ K, this analysis shows that the atomic states contain less than 10% of the excitation. Furthermore, these atomic states are not in equilibrium with the molecules (as noted in Sec. III.B, they are somewhat above their equilibrium values) and increasing the temperature tends to bring them closer to their equilibrium values (i.e., decreases the amount of energy stored in these states). Thus, even though the amount of energy wasted in the $^3P_0$ atomic metastables is rather small, this loss is also minimized by increasing the temperature.

We can now tabulate the 1_u excimer density and the gain as functions of temperature and the total excimer density n_{tot}. The gain is then calculated from Eqs. (5.3) and (5.4) and is given in Table IV as a function of n_{tot} and T. The numbers in parentheses represent the maximum permissible gas density for each case. The cases marked with an asterisk denote the fact that the gas density is limited by the condition that trimer losses be less than 10%, Eq. (5.5). For those cases with no asterisk, the gas density is limited by the condition that a 10 to 1 population inversion be maintained relative to the ground state, Eq. (5.7).

TABLE IV. The small signal gain at 335 nm is given in percent per meter as a function of gas temperature T and the total excimer density n_{tot}. Below each value of gain is the corresponding 1_u excimer density and, in parentheses, the maximum permissible gas density, both in cm^{-3}. For those cases marked by asterisk, the gas density is limited by trimer formation; for the cases with no asterisk, the gas density is limited by the condition that a 10% population inversion be maintained. For example, if the excimer density is 3×10^{15} at 1300 K, one obtains an excimer density of 1.2×10^{14} cm^{-3}, a gain of 1.6%/m, and a maximum permissible gas density of 3.7×10^{18} cm^{-3}. The gain is calculated with the expression $3.8\times10^{-16}\, n_{tot}\sqrt{T}\exp(-2534/kT)$ obtained from Eqs. (5.3) and (5.4).

n_{tot}	$T=1000$ K	$T=1300$ K	$T=2000$ K
3×10^{14}	0.094	0.25	0.82
	8.2×10^{12} (1.0×10^{18})	1.9×10^{13} (1.2×10^{18})	4.95×10^{13} (1.4×10^{18})
10^{15}	0.31	0.83	2.7
	2.7×10^{13} (1.7×10^{18})	6.3×10^{13} (2.0×10^{18})	1.65×10^{14} (2.4×10^{18})
3×10^{15}	0.94	2.5	8.2
	8.2×10^{13} (3.2×10^{18})	1.9×10^{14} (3.7×10^{18})	4.95×10^{14} (4.4×10^{18})
10^{16}	3.1	8.3	27.
	2.7×10^{14} (4.3×10^{18})*	6.3×10^{14} (6.5×10^{18})	1.65×10^{15} (7.5×10^{18})
3×10^{16}	9.4	25.	82.
	8.2×10^{14} (4.3×10^{18})*	1.9×10^{15} (1.2×10^{18})	4.95×10^{15} (1.4×10^{19})
10^{17}	31.	83.	270.
	2.7×10^{15} (4.3×10^{18})*	6.3×10^{16} (2.0×10^{19})	1.65×10^{16} (2.4×10^{19})
3×10^{17}	94.	250.	820.
	8.2×10^{15} (4.3×10^{18})*	1.9×10^{16} (3.7×10^{19})*	4.95×10^{16} (4.4×10^{19})

that trimer losses be less than 10%, Eq. (5.5). For those cases with no asterisk, the gas density is limited by the condition that a 10 to 1 population inversion be maintained relative to the ground state, Eq. (5.7).

In a 335 laser, a large amount of energy will be stored in the low lying metastable states 0_g^+. In order to convert this energy into 1_u molecules which produce the 335 nm emission, it is necessary to raise the vibrational temperature. In a conventional optically pumped laser, the vibrational temperature and the gas temperature will be the same. This means that, for reasonable temperatures $T<1300$ K, only 5% of the total excimer energy will be available for laser emission. However, in electrically excited lasers, it is possible to obtain vibrational temperatures which are much higher than the gas temperature (Mosburg and Wilke[7]). It is therefore quite reasonable to expect that a large fraction of the excimer energy can be converted into laser output.

In order to obtain gain on the 485 band one would want low temperatures and high densities. For densities above 3×10^{17} cm^{-3} and temperatures slightly above that which would produce condensation, essentially all the (optically produced) excimer energy channels through the 485 band. This gives almost 2 orders of magnitude improvement in energy extraction over a *low temperature* ($T<1300$ K) optically pumped 335 laser. On the other hand, the 485 band width is about 5 times wider and the A value may be 20 times smaller [Eq. (4.12)], resulting in a gain about 2 orders of magnitude lower than that for the 335 band. There may also be low lying metastable trimer states which will reduce the energy available for a 485 laser, and finally, there is a strong absorption near 485 nm in the dimer (Hill *et al.*[17] and Sec. IV of Drullinger *et al.*[1]). The prospects for a 485 laser thus seem less favorable than those for a 335 laser.

ACKNOWLEDGMENT

We would like to acknowledge many helpful discussions with Dr. A. V. Phelps of the Joint Institute for Laboratory Astrophysics.

APPENDIX: EMISSION AND ABSORPTION IN DIATOMIC EXCIMER MOLECULES

For a two-level absorber, the absorption coefficient is generally given by (Herzberg,[18] p. 383)

$$k_\nu = \frac{8\pi\nu}{3hc} f(\nu)\left(\frac{n_b}{d_b} - \frac{n_a}{d_a}\right)\sum_{ij} |\langle ai|D|bj\rangle|^2 \qquad \text{(A1)}$$

$$= \frac{c^2}{8\pi\nu^2} A_{ab} f(\nu)\left(\frac{d_a}{d_b} n_b - n_a\right) ,$$

where i and j denote *all* degenerate states for each level; a and b denote excited and ground electronic states; d_a and d_b are the degeneracy factors (i.e., the number of degenerate electronic, rotational, and vibrational states) for the levels a and b, respectively; $f(\nu)$ is a normalized line shape function; ν is the frequency in sec^{-1}; D is the transition dipole moment operator; and n_a and n_b are the population densities in the upper and lower states. The A value is defined by (Herzberg,[18] p. 21)

$$A_{ab} = \frac{64\pi^4\nu^3}{3hc^3}\sum_{ij}\frac{|\langle ai|D|bj\rangle|^2}{d_a}$$

$$= \frac{64\pi^4\nu^3}{3hc^3} g_b \sum_{ij}\frac{|\langle ai|D|bj\rangle|^2}{(2J+1)\omega_J} , \qquad \text{(A2)}$$

where g_b is the *electronic* degeneracy (assuming all degenerate electronic states have the same dipole matrix elements) and $(2J+1)\omega_J$ denotes the degeneracy of rotation vibration states. (ω_J is the nuclear degeneracy factor.)

The situation is slightly complicated for excimer molecules because several vibration–rotation states

can radiate at the same frequency and one must be careful to include their contributions correctly. We will therefore use $f(\nu) = \delta[\nu - (E_a - E_{vJ} - E_{v'J'})/h]$, where the energies E_{vJ} and $E_{v'J'}$ are measured from the bottom of their respective potential wells (we will allow for a shallow van der Waals well in the lower state) and sum over all vibration–rotation states. Our k_ν is given as

$$k_\nu = \frac{8\pi^3\nu}{3hc} \sum_{vJM,v'J'M'} \delta\left\{\nu - \frac{1}{h}(E_a + E_{vJ} - E_{v'J'})\right\} \times |\langle avJM|D|bv'J'M'\rangle|^2 \times\left(g_a \frac{n_{bv'J'}}{(2J'+1)\omega_{J'}} - g_b \frac{n_{avJ}}{(2J+1)\omega_J}\right). \quad \text{(A3)}$$

The sums over M and M' are readily performed by introducing the line strength $S_{JJ'}$ (Herzberg,[18] pp. 127 and 208) which has the property that $\sum_{J'} S_{JJ'} = \sum_{J} S_{J'J} = (2J+1)$:

$$\sum_{MM'} |\langle avJM|D|bv'J'M'\rangle|^2 = S_{JJ'} |\langle avJ|D|bv'J'\rangle|^2 . \quad \text{(A4)}$$

In this expression $|avJ\rangle$ and $|bv'J'\rangle$ denote vibrational wavefunctions (i.e., solutions of the radial Schrödinger equation).

In order to evaluate the ground state absorber density $n_{bv'J'}$, we consider the number of ground state atom pairs (i.e., bound as well as unbound molecules) which have an energy $E_{v'J'}$:

$$N_{bv'J'} = N^2(2J'+1)\omega_{J'} \frac{e^{-E_{v'J'}/kT}}{q} . \quad \text{(A5)}$$

The total number of ground state atoms is denoted by N; q is the partition function which includes contributions from bound and free states; and T is the gas temperature. Since the ground state well depth D_0 is very shallow (i.e., $D_0 < kT$), only a negligible fraction of ground state atom pairs will be bound. We thus use

$$q = \int d^3r \int d^3p\, e^{-p^2/2\mu kT} = \Omega\Lambda^{-3} e^{-D_0/kT} , \quad \text{(A6)}$$

where Ω denotes the volume of the system and Λ is the thermal de Broglie wavelength

$$\Lambda = \sqrt{h^2/2\pi\mu kT} . \quad \text{(A7)}$$

Equation (A5) thus becomes

$$n_{bv'J'} = n^2\Lambda^2(2J'+1)\omega_{J'} e^{-(E_{v'J'}-D_0)/kT} , \quad \text{(A8)}$$

where n is the ground state atom density. It is also convenient to transform the ground state vibrational wavefunctions into continuum states via the transformation (Mies[19])

$$|bv'J'\rangle = \sqrt{\frac{d\epsilon}{dv}}\, |b\epsilon J'\rangle \quad \sum_{v} \rightarrow \int d\epsilon \left(\frac{dv}{d\epsilon}\right) . \quad \text{(A9)}$$

Using Eqs. (A4), (A8), and (A9), the absorption coefficient becomes

$$k_\nu = \left(\frac{8\pi^3\nu}{3hc}\right) \sum_{vJJ'} \int d\epsilon\, \delta\left\{\nu - \frac{1}{h}(E_a + E_{vJ} - \epsilon)\right\} S_{JJ'} |\langle avJ|D|b\epsilon J'\rangle|^2 \left(g_a n^2\Lambda^3 e^{-(\epsilon - D_0)/kT} - g_b \frac{n_a e^{-E_{vJ}/kT_a}}{q_a}\right)$$
$$= \left(\frac{8\pi\nu}{3c}\right) \sum_{vJJ'} S_{JJ'} |\langle avJ|D|b\epsilon J'\rangle|^2 \left(g_a n^2\Lambda^3 e^{-E_{vJ}/kT} e^{-(E_a - D_0 - h\nu)/kT} - \frac{g_b n_a e^{-E_{vJ}/kT_a}}{q_a}\right) , \quad \text{(A10)}$$

where T_a is the vibrational temperature for the excited state, and n_a and q_a are the density and rotation–vibration partition function for excited molecules in the a state, again including (in principle) both bound and free states.

The dipole matrix element in Eq. (A10) can be expressed in terms of vibrational wavefunctions as

$$\langle avJ|D|b\epsilon J'\rangle = \int_0^\infty D_{ab}(R)\Psi^J_{av}(R)\Psi^{J'}_{b\epsilon}(R)\, dR , \quad \text{(A11)}$$

where $D_{ab}(R)$ denotes the dipole matrix element between the electronic states a and b. This integral can be evaluated using WKB wavefunctions,[20] in which case one finds that the integrand is sharply peaked about a critical radius R_ν at which the radial momenta for upper and lower states are equal (Franck–Condon principle):

$$\epsilon - V'_b(R_\nu) - \frac{\hbar^2 J'(J'+1)}{2\mu R_\nu^2} = E_{vJ} - V_a(R_\nu) - \frac{\hbar^2 J(J+1)}{2\mu R_\nu^2} , \quad \text{(A12)}$$

or, since $\epsilon = E_a + E_{vJ} - h\nu$,

$$h\nu = V_a(R_\nu) - \frac{\hbar^2 J(J+1)}{2\mu R_\nu^2} - V'_b(R_\nu) - \frac{\hbar^2 J'(J'+1)}{2\mu R_\nu^2}$$
$$\simeq E_a + V_a(R) - V'_b(R) , \quad \text{(A13)}$$

where V_a and V'_b equal zero at the bottoms of the excited state and ground state wells, respectively. In the last line of Eq. (A13) we have used the fact that the rotational levels with large thermal populations correspond to large J values, thus the $\Delta J = \pm 1, 0$ selection rule implies that the rotational energies essentially cancel out. That is, for a given vibrational level and a specific R_ν, all rotational levels emit photons of essentially the same frequency.

There is some rotational broadening due to the inexact cancellation of the rotational energies, but this is negligible for our purposes. Since the integrand in Eq. (A11) is sharply peaked at R_ν, the function D_{ab} may be factored out as $D_{ab}(R_\nu)$ and the remaining Franck–Condon overlap integral evaluated by the method of stationary phase. Mies[20] argues that the WKB phase integral (the integral over the radial momentum) for the repulsive state will be small (compared with π) at the point R_ν. Equation (A11) then reduces to

$$\langle avJ|D|b\epsilon J'\rangle = D_{ab}(R_\nu)\Psi^J_{av}(R_\nu)/\sqrt{(d/dR_\lambda)[V_a(R_\lambda) - V'_b(R_\lambda)]} . \quad \text{(A14)}$$

If the WKB phase integral is not small, Ψ_{av}^{J} is replaced by a slightly more complicated function of R_v. We must therefore emphasize that, for the high temperatures of interest to us ($T \gtrsim 400\,^{\circ}\mathrm{K}$) this phase integral will be small only if R_v lies near the classical turning point for the repulsive state (within 0.5 Å). This will be a good approximation since the WKB continuum wavefunction is sharply peaked about the classical turning point. In fact, one must be somewhat careful about using a WKB wavefunction for $\Psi_{av}^{J}(R_v)$, because the latter diverges at the turning point. However, Eq. (A14) can also be derived using Airy wavefunctions which do not diverge[21]; hence one can readily find well-behaved wavefunctions for use with this expression. It should be noted that Eq. (A14) is quite similar to the "reflection method" (Herzberg,[18] p. 392) in which the repulsive state wavefunction is replaced by a delta function at the classical turning point. It should also be noted that Eq. (A14) breaks down if the derivative of $(V_a - V_b)$ should vanish at R_λ; in such a case one must use a higher order stationary phase integration. We next note that the vibrational wavefunction Ψ_{av}^{J} depends on J only through the radial kinetic energy $E_{vJ} - V_a(R) - \hbar^2 J(J+1)/2\mu R^2$. Since for not too large values of J the shape of the potential energy curve $V_a(R) + \hbar^2 J(J+1)/2\mu R^2$ does not differ appreciably from that of $V_a(R)$, we will approximate the rotational energy $\hbar^2 J(J+1)/2\mu R^2$ by using $R \simeq R_v$. This approximation ignores a small distortion produced by the rotational energy, but this should be negligible for our purposes.[22] Therefore, if we replace E_{vJ} in Eq. (A10) by

$$E_{vJ} = E_v + \frac{\hbar^2 J(J+1)}{2\mu R_v^2} \quad , \tag{A15}$$

the radial energy becomes $E_{vJ} - V_a(R) - \hbar^2 J(J+1)/2\mu R^2 \simeq E_v - V_a(R)$, and the vibrational wavefunction Ψ_{avJ} becomes simply Ψ_{av} since it no longer depends on J. Using Eqs. (A14) and (A15) we may perform the sum over J' in Eq. (A10) which yields $(2J+1)$. We thus obtain

$$k_v = \frac{8\pi^3 \nu}{3c} \left|D_{ab}(R)\right|^2 \frac{1}{h(d\nu/dR)} \sum_v \left|\psi_{av}(R_v)\right|^2 \sum_J (2J+1)$$
$$\times \left(g_a n^2 \Lambda^3 e^{-J(J+1)\hbar^2/2\mu R_v^2 kT} e^{-E_{v'}/kT} e^{[V_a(R_v) - V_b'(R_v) + D_0]/kT} - \frac{g_b n_a}{q_a} e^{J(J+1)\hbar^2/2\mu R_v^2 kT_a} e^{-E_v/kT_a} \right) , \tag{A16}$$

where we have replaced $d(V_a - V_b')/dR_v$ by $h(d\nu/dR)$ using Eq. (A13). The sum over J is converted into an integral which yields $4\pi R_v^2/\Lambda^2$. The sum over v is performed using harmonic oscillator wavefunctions with a force constant $\alpha = \mu\omega/\hbar$ [Merzbacher[23] and Bateman[24] identity (22), p. 194]:

$$\sum_v \left|\psi_{av}(R_v)\right|^2 e^{-E_v/kT} = \sum_n \sqrt{\frac{\alpha}{\pi}} \frac{1}{2^n n'} e^{-\alpha R^2} H_n^2(\sqrt{\alpha} R)\, e^{-\hbar\omega(n+1/2)/kT} = \sqrt{\frac{\alpha kT}{2\pi\hbar\omega}}\, e^{-\mu\omega^2 R_v^2/2kT} = \Lambda^{-1} e^{-V_a(R_v)/kT} \quad . \tag{A17}$$

This result represents the contribution from both bound and free states assuming complete thermal equilibrium; it can also be derived using WKB wavefunctions which are more appropriate for free states. In any case, the contribution from the free states is negligible since it is proportional to $\exp(-D/kT)$, where $D \sim 800\ \mathrm{cm}^{-1}$ is the dissociation energy of the $^3\Pi_u$ state. For simplicity we define a ground state potential function

$$V_b(R) = V_b'(R) - D_0 \tag{A18}$$

which goes to zero as $R \to \infty$. Equation (A16) now becomes

$$k_v = \left(\frac{8\pi^3 \nu}{3hc}\right) \left|D_{ab}(R_v)\right|^2 \frac{4\pi R_v^2}{(d\nu/dR_v)} \left(q_a n^2 e^{-V_b(R_v)/kT} - \frac{g_b n_a}{\Lambda_a^3 q_a} e^{-V_a(R_v)/kT_a} \right)$$
$$= \frac{c^2}{8\pi\nu^2} A_{ab}(\nu)\phi(\nu) \left(\frac{g_a n^2}{g_b} e^{-V_b(R_v)/kT} - \frac{n_a}{q_a \Lambda_a^3} e^{-V_a(R_v)/kT_a} \right) , \tag{A19}$$

where Λ_a is a de Broglie wavelength at the temperature T_a [cf. Eq. (A7)] and

$$A_{ab}(\nu) = (64\pi^4 \nu^3/3hc^3) g_b \left|D_{ab}(R_v)\right|^2 . \tag{A20}$$

$\phi(\nu)$ is an unnormalized line shape function defined by

$$\phi(\nu) = 4\pi R_v^2 \frac{dR_v}{d\nu} \quad . \tag{A21}$$

One could define normalized emission and absorption line shape functions

$$f_A(\nu) = \phi(\nu)\, e^{-V_b(R_v)/kT} \left(\int d^3R e^{-V_b(R)/kT} \right)^{-1} ,$$
$$f_E(\nu) = \phi(\nu)\, e^{-V_a(R_v)/kT} \left(\int d^3R\, e^{-V_a(R)/kT_a} \right)^{-1} , \tag{A22}$$

but for our purposes, Eq. (A19) is more convenient as it stands.

The total number of photons emitted into 4π steradians per unit frequency interval is evaluated in exactly the same way as Eqs. (A1)–(A19). It is given by

$$I(\nu)d\nu = A_{ab}(\nu)\phi(\nu) \frac{N_a e^{-V_a(R_v)/kT_a}}{\Lambda_a^3 q_a} d\nu \quad . \tag{A23}$$

Since our data are scaled in wavelength, we will use

$$I(\lambda)d\lambda = A_{ab}(\lambda)\phi(\lambda) \frac{N_a e^{-V_a(R_\lambda)/kT_a}}{\Lambda^3 q_a} \left(\frac{c}{\lambda^2}\right) d\lambda , \tag{A24}$$

$$k(\lambda) = \left(\frac{\lambda^2}{8\pi}\right) A_{ab}(\lambda)\phi(\lambda) \times \left(\frac{g_a n^2}{g_b} e^{-V_b(R_\lambda)/kT} - \frac{N_a}{\Lambda_a^3 q_a} e^{-V_a(R_\lambda)/kT_a}\right). \quad \text{(A25)}$$

*Supported in part by ERDA Contract No. E(49-1)-3800 and by ARPA Order No. 891. Amendment 11.

†Joint Institute for Laboratory Astrophysics and Department of Physics and Astrophysics, University of Colorado.

[1]R. E. Drullinger, M. M. Hessell, and E. W. Smith, J. Chem. Phys. 66, 5656 (1977), previous paper.
[2]H. Kuhn and K. Freudengerg, Z. Phys. 76, 38 (1932).
[3]K. M. Sando and J. C. Wormhoudt, Phys. Rev. A 7, 1889 (1973).
[4]R. E. M. Hedges, D. L. Drummond, and A. Gallagher, Phys. Rev. 6, 1519 (1972).
[5]R. O. Doyle, J. Quant. Spectrosc. Radiat. Transfer 8, 1555, (1968).
[6]K. M. Sando and A. Dalgarno, Mol. Phys. 20, 103 (1971).
[7]E. R. Mosburg and M. Wilke, J. Chem. Phys. 66, 5682 (1977), following paper.
[8]R. E. Drullinger, M. M. Hessel, and E. W. Smith, Natl. Bur. Stand. Monograph 143 (1975).
[9]W. J. Stevens (private communication).
[10]F. Mies, M. Krauss, and W. J. Stevens (work in progress).
[11]W. Baylis and Walorny) (work in progress).
[12]K. Kuhn, Proc. R. Soc. London 158, 230 (1937).
[13]J. Frank and W. Grotrian, Z. Tech. Phys. 3, 194 (1922).
[14]E. Koernieke, Z. Phys. 33, 219 (1925).
[15]D. Perrin-Lagarde and R. Lennuier, J. Phys. (Paris) 36, 357 (1975).
[16]N. Davidson, *Statistical Mechanics* (McGraw-Hill, New York, 1962).
[17]R. M. Hill, D. J. Eckstrom, D. C. Lorents, and H. H. Nakano, Appl. Phys. Lett. 23, 373 (1973).
[18]G. Herzberg, *Molecular Spectra and Molecular Structure* (Van Nostrand Reinhold, New York, 1950), 2nd ed.
[19]F. H. Mies, Mol. Phys. 26, 1233 (1973).
[20]F. H. Mies, J. Chem. Phys. 48, 482 (1968).
[21]W. H. Miller, J. Chem. Phys. 48, 464 (1968).
[22]G. E. Gibson, O. K. Rice, and N. S. Bayliss, Phys. Rev. 44, 193 (1933).
[23]E. Merzbecher, *Quantum Mechanics* (Wiley, New York, 1962).
[24]H. Bateman Manuscript Project, *Higher Transcendental Functions* (McGraw-Hill, New York, 1953), Vol. 2.
[25]C. G. Matland and A. O. McCoubrey, unpublished Westinghouse Research Memo.
[26]The fluorescence intensity was obtained with a spectrometer and phototube which were calibrated using a standard lamp.[1] The intensity plotted is proportional to the number of photons emitted per unit wavelength.